Cellular/Molecular

Membrane Trafficking of NADPH Oxidase p47^{phox} in Paraventricular Hypothalamic Neurons Parallels Local Free Radical Production in Angiotensin II Slow-Pressor Hypertension

Christal G. Coleman,[1] Gang Wang,[1] Giuseppe Faraco,[1] Jose Marques Lopes,[1] Elizabeth M. Waters,[2] Teresa A. Milner,[1,2] Costantino Iadecola,[1] and Virginia M. Pickel[1]

[1]Brain and Mind Research Institute, Weill Cornell Medical College of Cornell University, New York, New York 10065, and [2]Harold and Margaret Milliken Hatch Laboratory of Neuroendocrinology, The Rockefeller University, New York, New York 10065

NADPH oxidase-generated reactive oxygen species (ROS) are highly implicated in the development of angiotensin II (AngII)-dependent hypertension mediated in part through the hypothalamic paraventricular nucleus (PVN). This region contains vasopressin and non-vasopressin neurons that are responsive to cardiovascular dysregulation, but it is not known whether ROS is generated by one or both cell types in response to "slow-pressor" infusion of AngII. We addressed this question using ROS imaging and electron microscopic dual labeling for vasopressin and p47^{phox}, a cytoplasmic NADPH oxidase subunit requiring mobilization to membranes for the initiation of ROS production. C57BL/6 mice or vasopressin-enhanced green fluorescent protein (VP–eGFP) mice were infused systemically with saline or AngII (600 ng · kg^{-1} · min^{-1}, s.c.) for 2 weeks, during which they slowly developed hypertension. Ultrastructural analysis of the PVN demonstrated p47^{phox} immunolabeling in many glial and neuronal profiles, most of which were postsynaptic dendrites. Compared with saline, AngII recipient mice had a significant increase in p47^{phox} immunolabeling on endomembranes just beneath the plasmalemmal surface (+42.1 ± 11.3%; $p < 0.05$) in non-vasopressin dendrites. In contrast, AngII infusion decreased p47^{phox} immunolabeling on the plasma membrane (−35.5 ± 16.5%; $p < 0.05$) in vasopressin dendrites. Isolated non-VP–eGFP neurons from the PVN of AngII-infused mice also showed an increase in baseline ROS production not seen in VP–eGFP neurons. Our results suggest that chronic low-dose AngII may offset the homeostatic control of blood pressure by differentially affecting membrane assembly of NADPH oxidase and ROS production in vasopressin and non-vasopressin neurons located within the PVN.

Introduction

Angiotensin II (AngII) is an important mediator of neurogenic hypertension and has been suggested to increase blood pressure by enhancing production of reactive oxygen species (ROS) (Infanger et al., 2006; Peterson et al., 2006; Braga et al., 2011). Chronic systemic (Kang et al., 2009) or acute central (Erdös et al., 2006) AngII administration increases ROS production in the hypothalamic paraventricular nucleus (PVN). This brain region is a critical integration site for neuronal pathways involved in cardiovascular regulation mediated through neurohumoral outputs to the pituitary and descending neural projections to sympathoregulatory neurons in the brainstem and spinal cord (Benarroch, 2005; Biag et al., 2012).

Received June 28, 2012; revised Dec. 10, 2012; accepted Jan. 9, 2013.

Author contributions: C.G.C. and V.M.P. designed research; C.G.C., G.W., G.F., and J.M.L. performed research; E.M.W. and T.A.M. contributed unpublished reagents/analytic tools; C.G.C., G.W., C.I., and V.M.P. analyzed data; C.G.C. wrote the paper.

This work was supported by National Institutes of Health Grants HL096571 (V.M.P., C.I.) and HL098351 (T.A.M.).

Correspondence should be addressed to Dr. Virginia M. Pickel, 407 East 61st Street, Third Floor, New York, NY 10065. E-mail: vpickel@med.cornell.edu.

DOI:10.1523/JNEUROSCI.3061-12.2013

 0270-6474/13/334308-09$15.00/0

AngII-induced blood pressure elevation and enhanced ROS production in the PVN can be attenuated by central administration of NADPH oxidase inhibitors (Erdös et al., 2006). These findings are similar to those in brainstem autonomic regions (Wang et al., 2004, 2006), which collectively suggest a causative role of NADPH oxidase-generated ROS in the development of AngII-dependent hypertension. This may include the slow-pressor hypertension resulting from chronic systemic infusion of a subpressor dose of AngII, as has been shown in peripheral blood vessels (Kawada et al., 2002).

NADPH oxidase is a multicomponent enzyme complex in central autonomic hypothalamic neurons (Infanger et al., 2006). NADPH oxidase consists of a membrane-associated cytochrome (p22^{phox} and gp91^{phox}) and cytoplasmic (p40^{phox}, p47^{phox}, and p67^{phox}) proteins (Bedard and Krause, 2007). For ROS production, the NOX2 isoform of NADPH oxidase requires mobilization of cytoplasmic p47^{phox} to assimilate with the membrane-bound proteins (Jones et al., 1994). Thus, the analysis of the subcellular distribution of p47^{phox} may provide critical insight as to whether NOX2 is activated in specific subpopulations of hypothalamic neurons. This powerful approach has not yet been used in conjunction with slow-pressor AngII hypertension, although there is

evidence for gp91^{phox} (NOX2) and p47^{phox} upregulation in the PVN of rats with renovascular hypertension (Oliveira-Sales et al., 2009).

Circulating AngII acts centrally to not only increase the excitability of PVN neurons modulating sympathetic outflow but also to stimulate vasopressin release from PVN neurons (Keil et al., 1975; Veltmar et al., 1992; Capone et al., 2012). The vasopressin neurons are highly sensitive to disturbances of cardiovascular and fluid homeostasis (de Wardener, 2001; Kc et al., 2010) but do not express AngII type 1 (AT1) receptors (Gonzalez et al., 2012) that are major mediators of AngII-induced oxidative stress responses (Qi et al., 2013). Thus, vasopressin neurons may not be among those cells that have the capacity to respond to chronic AngII by producing NADPH oxidase-generated ROS. To test this hypothesis, we used ROS imaging in whole-brain sections and dissociated cells to determine the effect of slow-pressor systemic infusion of AngII on ROS production in PVN neurons distinguished by their vasopressin content. In addition, using an ultrastructural approach, we sought to determine whether (1) vasopressin-containing neurons express p47^{phox} and (2) chronic infusion of subpressor doses of AngII induces p47^{phox} membrane trafficking in vasopressin and/or non-vasopressin neurons in the mouse PVN.

Materials and Methods

Animals. Experimental procedures were approved by the Institutional Animal Care and Use Committee of Weill Cornell Medical College and were in accordance with the 2011 Eighth Edition of the National Institute of Health *Guide for the Care and Use of Laboratory Animals*. The studies were conducted in adult male C57BL/6 mice (9–10 weeks; 25–30 g), obtained from The Jackson Laboratory and vasopressin-enhanced green fluorescent protein (VP–eGFP) mice on a C57BL/6 background (9–10 weeks; 25–30 g). The VP–eGFP mice were originally developed by the Rockefeller GENSAT Project (Gong et al., 2003) and bred at Rockefeller University.

AngII administration. Osmotic mini-pumps (Alzet) containing vehicle (saline) or AngII (600 ng · kg^{-1} · min^{-1}) were implanted subcutaneously in mice under isoflurane anesthesia. At the end of the 14 d experimental period, systolic blood pressure was measured in awake mice by tail-cuff plethysmography, as described previously (Coleman et al., 2010).

ROS detection in vivo. ROS production was determined using *in vivo* dihydroethidium (DHE) microfluorography, as described previously (Kunz et al., 2007). DHE is a cell-permeant dye that is oxidized to ethidium (Eth) and related products by superoxide. Eth is trapped intracellularly by intercalating with DNA (Rothe and Valet, 1990). The fluorescence signal attributable to DHE oxidation products reflects cumulative ROS production during the period between administration of DHE and killing the animal. After 14 d of infusion with either saline ($n = 8$ mice per /group) or AngII ($n = 8$ mice per group), mice were anesthetized with isoflurane (5% induction; 2% maintenance), and DHE (10 mg/kg) was injected into the jugular vein. Four hours later, the animals were killed, and the brains were rapidly removed and frozen. Brains from both treatment groups were coprocessed under identical conditions. Coronal sections cut on the cryostat (20 μm thickness) were mounted on gelatin-coated slides, and the Eth fluorescence signals in the PVN were examined using a Leica TCS SP5 confocal microscope (Leica Microsystems) with laser excitation at 488 nm. All images were obtained using the same confocal settings. To assess ROS production in PVN neurons, Eth fluorescence was quantified using NIH ImageJ. Fluorescence data are expressed in arbitrary units.

ROS detection in vitro. ROS production was assessed in isolated PVN neurons from mice infused with saline ($n = 5$ mice per group) or slow-pressor doses of AngII ($n = 5$ mice per group) over a period of 14 d. The mice were anesthetized with CO_2, and their brains were removed and immersed in ice-cold sucrose–artificial CSF (aCSF) composed of the following (in mM): 26 $NaHCO_3$, 1 NaH_2PO_4, 3 KCl, 5 $MgSO_4$, 0.5 $CaCl_2$, 10 glucose, and 248 sucrose, pH 7.4 (oxygenated with 95% O_2 and 5% CO_2). Coronal slices (300 μm thickness) containing the PVN were obtained using a vibratome and stored in oxygenated lactic acid (l)-aCSF composed of the following (in mM): 124 NaCl, 26 $NaHCO_3$, 5 KCl, 1 NaH_2PO_4, 2 $MgSO_4$, 2 $CaCl_2$, 10 glucose, and 4.5 lactic acid, pH 7.3 (at 35°C for 1 h). The PVN slices were then incubated at 35°C with 0.02% Pronase and thermolysin (Sigma-Aldrich) in l-aCSF gassed with 95% O_2 and 5% CO_2 for 2 h. The tissue slices were micropunched under a dissecting microscope to remove the PVN region, and cells were dissociated by mechanical stirring. Dissociated PVN cells were transferred to a poly-L-lysine-coated, glass-bottomed Petri dish and were perfused with a modified Mg^{2+}-free l-aCSF containing the following (in mM): 121 NaCl, 5 KCl, 1.8 $CaCl_2$, 0.01 glycine, 1 Na-pyruvate, 20 glucose, 26 $NaHCO_3$, 1 NaH_2PO_4, and 4.5 lactic acid, pH 7.4 (95% O_2 and 5% CO_2). Neurons were identified based on their morphology, presence of processes, and positivity for VP–eGFP using FITC filter (Chroma Technology).

Methods for ROS detection in isolated cells using DHE have been described in detail previously (Girouard et al., 2009) and are briefly summarized. Isolated PVN cells were incubated in DHE (2 μmol/L) for 30 min. Time-resolved fluorescence using Eth bromide filter (Chroma Technology) was measured at 1 min intervals with a Nikon diaphot 300 inverted microscope equipped with a CCD digital camera (Princeton Instruments) and IPLab software (Scanalytics). Recordings were started after a stable baseline measurement was achieved, usually within 10 min. The Eth fluorescence signals in PVN cells were recorded with bath application of either vehicle (saline) or 100 μM NMDA, a substance that is known to induce NOX2-dependent free radical production in the brain (Girouard et al., 2009). Eth fluorescence data are expressed in arbitrary units. A two-way ANOVA followed by Tukey's *post hoc* test was used for statistical comparisons between saline, AngII, or vehicle and NMDA groups. Differences were considered statistically significant when $p \leq 0.05$.

Antisera. For labeling of p47^{phox}, we used goat polyclonal antiserum (catalog #sc-7660; Santa Cruz Biotechnology) raised against a peptide mapping at the C terminal of human p47^{phox}. Western blot analysis has shown that this affinity-purified antibody specifically recognizes a band of ~47 kDa in lysate from HEK293T cells transfected with the p47^{phox} gene (Santa Cruz Biotechnology). The specificity of the p47^{phox} antiserum was tested using brain sections containing the PVN from p47^{phox} (+/+) wild-type (WT) and p47^{phox} (−/−) knock-out [KO; strain: B6(Cg)-Ncf1^{m1J}/J; The Jackson Laboratory] mice. In acrolein/paraformaldehyde-perfused WT tissue, p47^{phox} immunolabeling was observed in perikarya and processes throughout the PVN, whereas no visible immunolabeling was seen in this region in similarly processed tissue from the KO mice (data not shown).

For labeling of vasopressin, we used a polyclonal antiserum that was generated in guinea pig (catalog #T-5048; Peninsula Laboratories). Radioimmunoassay has shown this antiserum to have complete recognition of vasopressin, a slight cross-reaction (<0.1%) with other vasopressin derivatives, and no recognition of oxytocin (Peninsula Laboratories Technical Services). No immunolabeling was seen using this antiserum in Brattleboro rats, which do not express vasopressin (Drouyer et al., 2010).

Tissue preparation. Mice were deeply anesthetized with sodium pentobarbital (100 mg/kg, i.p.) and perfused through the left ventricle of the heart sequentially with 5–10 ml of heparin–saline, 30 ml of 3.75% acrolein in 2% paraformaldehyde, and 100 ml of 2% paraformaldehyde in 0.1 M phosphate buffer (PB), pH 7.4. AngII-treated ($n = 5$) and saline-treated ($n = 5$) mice were perfused with the same batch of solutions. The brains were removed, cut into thick coronal slices (~2 mm) using a mouse brain mold (Activational Systems) and postfixed in 2% paraformaldehyde for 30 min at room temperature. The tissue then was cut (40 μm thick) through the region of the PVN (0.70–0.94 mm) caudal to bregma (Paxinos and Franklin, 2001) using a vibratome (Leica Microsystems). Before immunocytochemistry, sections from control and experimental mice were uniquely identified by hole punches and placed in a single crucible containing PB (Milner et al., 2011). The free-floating

acrolein-fixed tissue sections were treated with 1% sodium borohydride in 0.1 M PB for 30 min to neutralize reactive aldehydes.

Electron microscopic immunocytochemistry. Tissue sections were processed using a preembedding dual immunolabeling protocol, as described previously (Lane et al., 2008; Coleman et al., 2010). Briefly, the sections were incubated in a cryoprotectant solution (25% sucrose and 3% glycerol in 0.05 M PB) for 15 min at room temperature, followed by an additional incubation in the cryoprotectant solution for 20 min at −80°C. The frozen tissue was thawed, rinsed, and placed in 0.5% bovine serum albumin (BSA) in 0.1 M Tris-buffered saline (TBS) for 30 min to minimize nonspecific binding of the antisera. The tissue was incubated for 24 h at room temperature in a solution of goat anti-p47^{phox} (1:50 dilution) and guinea pig anti-vasopressin (1:4000 dilution) antisera in 0.1 M TBS with 0.1% BSA.

For immunoperoxidase detection of vasopressin, sections were placed for 30 min in goat anti-guinea pig IgG (1:400; Jackson ImmunoResearch), followed by a 30 min incubation in avidin–biotin complex (Vector Laboratories). The bound peroxidase was visualized by reaction of the sections for 5–6 min in 3,3′-diaminobenzidine (DAB; Sigma-Aldrich) and hydrogen peroxide.

For immunogold detection of p47^{phox}, the DAB-reacted sections were rinsed and placed for 2 h in a 1:50 dilution of donkey anti-goat IgG with bound 1 nm colloidal gold (Electron Microscopy Sciences). The gold particles were fixed to the tissue in 2% glutaraldehyde, and the bound silver–gold particles were enhanced using a Silver IntenSEM kit (RPN491; GE Healthcare) for 7 min.

Tissue sections were postfixed in 2% osmium tetroxide for 1 h and then dehydrated through a series of graded ethanols and propylene oxide and flat-embedded in Embed-812 (Electron Microscopy Sciences) between two sheets of Aclar plastic.

Sectioning and ultrastructural data analyses. Ultrathin sections (70 nm thickness) from the PVN were cut with a diamond knife (Electron Microscopy Sciences) using a Leica EM UC6 ultratome (Leica Microsystems). The sections were collected on 400-mesh thin-bar copper grids (Electron Microscopy Sciences), counterstained with uranyl acetate and lead citrate, and examined using a Philips CM10 transmission electron microscope (FEI). Microscopic images were captured with an AMT Advantage HR/HR-B CCD camera system (Advanced Microscopy Techniques). Seventy-five to 100 microscopic images at a magnification of 19,000× were taken per animal.

Ultrastructural analysis was done exclusively on tissue collected from the surface to minimize differences in immunolabeling attributable to differential penetration of reagents in deeper tissue (Milner et al., 2011). An equal amount of tissue from each treatment group (9596 μm^2/treatment) was sampled for electron microscopic analysis. Profiles containing p47^{phox} or vasopressin immunoreactivity were classified as neuronal (soma, dendrites, axons, terminals) or glial based on criteria described by Peters et al. (1991). Dendrites were identified by the prevalence of endoplasmic reticulum and/or synaptic inputs from vesicle-filled axon terminals. Dendritic profiles were considered to be selectively labeled when they contained two or more gold particles. Small glial and axonal profiles (<0.4 μm) were considered immunogold labeled when containing only one gold particle. Peroxidase-immunoreactive profiles displayed a granular, electron-dense precipitate unlike the lighter, homogenous density of myelinated axons and other lipid-enriched membranes seen within the neuropil.

The p47^{phox} immunogold particles in the 14 d saline and AngII treatment groups were quantitatively compared in dendritic profiles with or without peroxidase immunoreaction product for vasopressin in the PVN. The shortest distance from the center of each gold particle to the plasma membrane was measured using Microcomputer Image Device software (MCID; Imaging Research). Additionally, MCID was used to determine the cross-sectional diameter, perimeter, surface area, and form factor of each immunolabeled dendrite. A cluster analysis (SPSS) was performed to divide the dendrites into size categories so that dendrites within a specific size range could be compared across treatment groups. Dendrites with an oblong or irregular shape (form factor value <0.5) were excluded from the dataset. Immunogold particles within dendrites were counted and categorized as (1) contacting the plasma membrane, (2) close to the plasma membrane (particles not touching but within 70 nm from the plasma membrane), or (3) cytoplasmic. Each digital electron microscopic image was blind coded so the investigator performing the quantification of gold particles was unaware of the treatment.

The parameters used for statistical comparisons were as follows: (1) the number of plasmalemmal p47^{phox} gold particles on a dendrite/dendritic perimeter, (2) the number of p47^{phox} gold particles close to the plasma membrane/dendritic perimeter, (3) the number of cytoplasmic p47^{phox} gold particles/dendritic cross-sectional area, and (4) the total p47^{phox} gold particles (plasmalemmal plus cytoplasmic) in a dendrite/dendritic cross-sectional area. Single-labeled (p47^{phox}) and dual-labeled (p47^{phox}/vasopressin) dendrites were analyzed separately. The measures of gold particle density were evaluated using a two-way (treatment × dendritic size) ANOVA, followed by a *post hoc* analysis using Tukey's test. Data are expressed as means ± SEM for the experimental and control groups of animals. The gold particle association with intracellular membranes was evaluated using a χ^2 test. Values were considered to be statistically significant when $p \leq 0.05$.

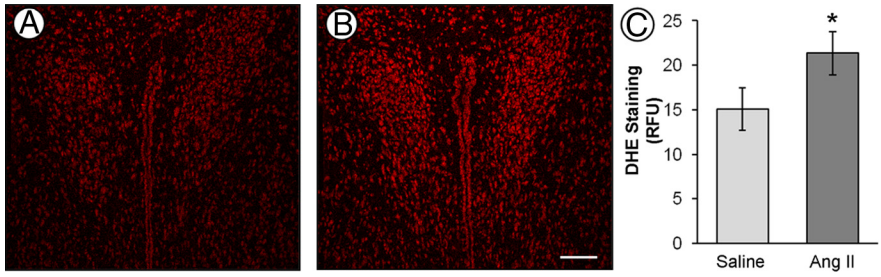

Figure 1. Representative images of ROS-dependent DHE fluorescence in the PVN of saline (***A***) and AngII (***B***) recipient mice. Compared with saline control, slow-pressor doses of AngII increases ROS production in the PVN (***C***; $n = 8$ mice per group). *$p <$ 0.05. Scale bar, 100 μm.

Results

Slow-pressor AngII infusion elevates blood pressure and induces ROS production in the hypothalamic PVN

A significant increase ($t_{(24)=}$ 5.79; $p < 0.001$) in systolic arterial blood pressure was observed in AngII-infused mice (141 ± 3 mmHg) compared with the saline-infused mice (111 ± 4 mmHg) after 14 d. These findings correspond well with telemetric blood pressure measurements obtained previously in mice receiving an identical dose of AngII (600 ng · kg^{-1} · min^{-1}) (Capone et al., 2011). Using DHE microfluorography in brain sections, we found that ROS generation was elevated ($t_{(14)=}$ 1.84; $p < 0.05$) in the PVN after AngII treatment (Fig. 1).

Chronic AngII differentially affects ROS production in isolated PVN VP–eGFP and non-VP–eGFP neurons

ROS-sensitive dye was seen by fluorescence imaging in many isolated PVN neurons recognizable by their ramifying processes (Fig. 2*A*). These neurons included those with or without VP–eGFP. Only the non-VP–eGFP neurons showed baseline levels of ROS that were significantly ($p < 0.05$) greater in the AngII compared with saline recipient mice (Fig. 2*B*). However, in both cell types, ROS levels were enhanced by bath application of NMDA, and the NMDA-evoked ROS was significantly greater in neurons isolated from mice receiving systemic AngII compared with saline (Fig. 2*B*,*C*).

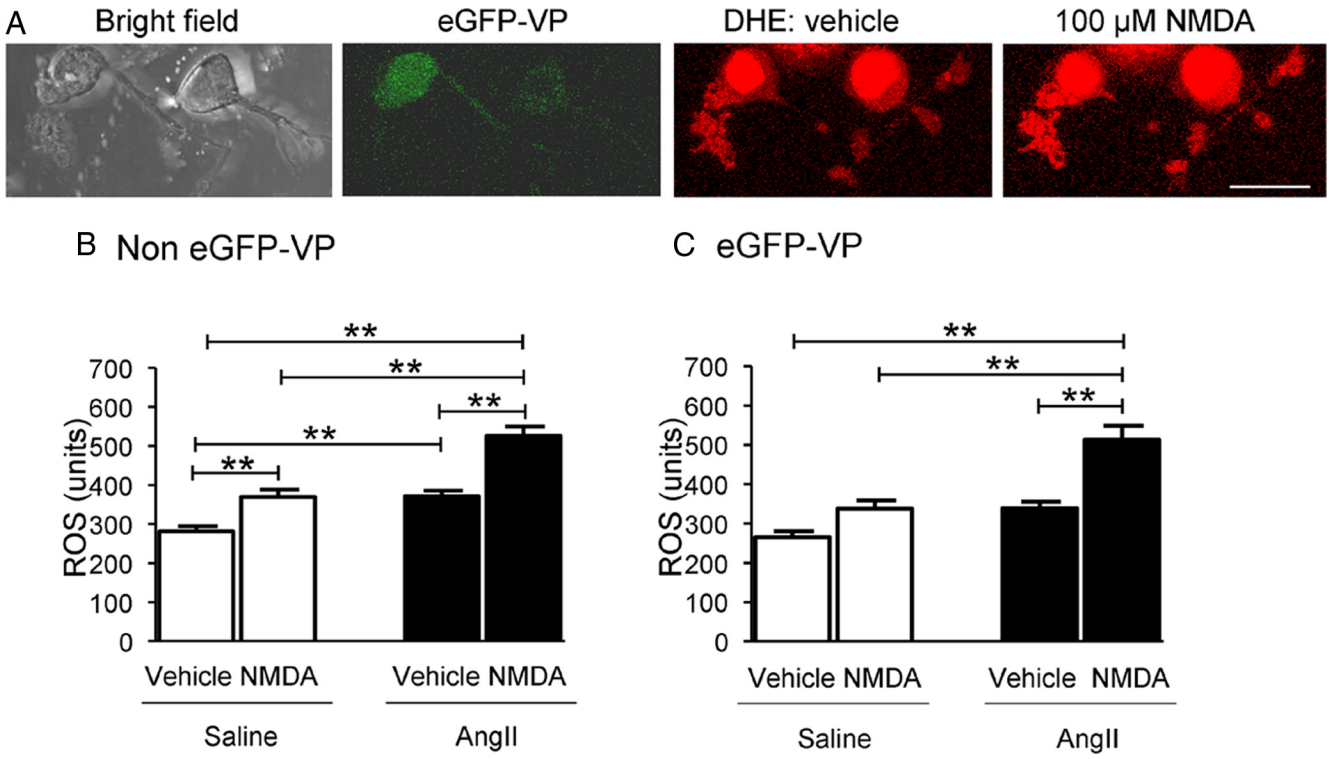

Figure 2. Comparisons of baseline ROS levels and NMDA-triggered ROS production between saline- and AngII-infused PVN cells. ***A***, Representative images of bright-field and VP– eGFP cells (green) and ROS-dependent Eth fluorescence (red) of these cells before and after the application of NMDA from an animal infused with AngII for 14 d. ***B***, In non-VP– eGFP PVN cells ($n = 21$ in saline and 20 in AngII groups), NMDA (100 μM) significantly increases ROS production in both saline ($31.5 \pm 4.9\%$; $p < 0.01$) and AngII ($41.8 \pm 4.5\%$; $p < 0.01$) groups (also $p < 0.01$ for AngII vs saline groups). In addition, AngII infusion significantly increases the baseline ROS level in non-VP– eGFP PVN cells ($+31.9 \pm 3.9$; $p < 0.01$ vs saline infusion). ***C***, In VP– eGFP PVN cells ($n = 16$ in saline and 14 in AngII groups), NMDA does not significantly increase ROS production in the saline group, but it does significantly increase ROS production in the AngII group ($+51.4 \pm 6.7\%$; $p < 0.01$) (also $p < 0.01$ for AngII vs saline groups). AngII infusion does not significantly enhance the baseline ROS level in VP– eGFP cells ($p > 0.05$ vs saline infusion). Scale bar, 20 μm. **$p < 0.01$.

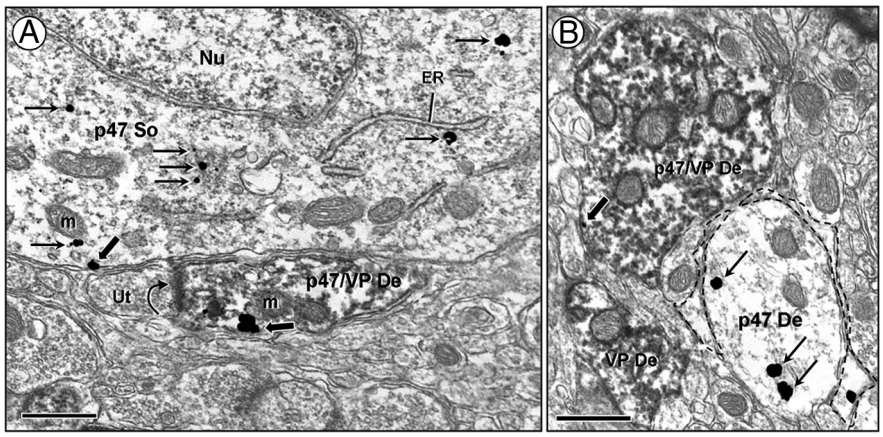

Figure 3. Electron microscopic images illustrating immunogold labeling for p47^{phox} in neuronal and glial processes in the PVN. ***A***, In somata (p47 So), p47^{phox} is found on the plasma membrane and in the cytoplasm near endoplasmic reticulum (ER) and mitochondria (m). The p47^{phox}-labeled soma is adjacent to a dendrite (p47/VP De) containing p47^{phox} and vasopressin immunoreactivity. The peroxidase vasopressin labeling is diffusely distributed throughout the cytoplasm. A cluster of p47^{phox} immunogold is found on the plasma membrane of this dual-labeled dendrite receiving an asymmetric excitatory-type synaptic contact (curved arrow) from an unlabeled terminal (Ut). ***B***, A p47 De is surrounded by a thin p47^{phox}-labeled glial process (dashed outline). A single-labeled (VP De) and dual-labeled (p47/VP De) dendrite is found in the nearby neuropil. Nu, Nucleus. Scale bar, 500 nm.

Immunogold p47^{phox} labeling in the PVN is predominantly localized to somatodendritic and glial profiles

Electron microscopy of the PVN revealed the presence of p47^{phox} in neuronal somata and dendrites with and without vasopressin immunoreactivity. In somata, the p47^{phox} immunogold labeling was evident near intracellular organelles, such as mitochondria and endoplasmic reticulum, and on the plasma membrane (Fig. 3*A*). A similar labeling pattern was seen in dendrites (Fig. 3*A*,*B*), and these dendrites accounted for the majority of all p47^{phox} immunolabeled profiles in control animals (568 of 747). The p47^{phox} immunogold particles were less frequently observed in axons (18 of 747) and axon terminals (47 of 747).

In addition to the neuronal distribution, p47^{phox} immunogold particles also were located in glia (114 of 747; Figs. 3*B*, 4). The p47^{phox} immunogold was present both in the cytoplasm and along the membrane of glial processes. p47^{phox}-containing glia included those having perisynaptic as well as perivascular distributions. Vasopressin immunoreactivity was not coexpressed with p47^{phox} labeling in glia.

Basal distribution for p47^{phox} is similar in dendrites with or without vasopressin

A small population of neuronal profiles in the PVN contained both p47^{phox} and vasopressin immunoreactivities. Of all p47^{phox}-labeled dendrites, 18% (102 of 568) coexpressed vaso-

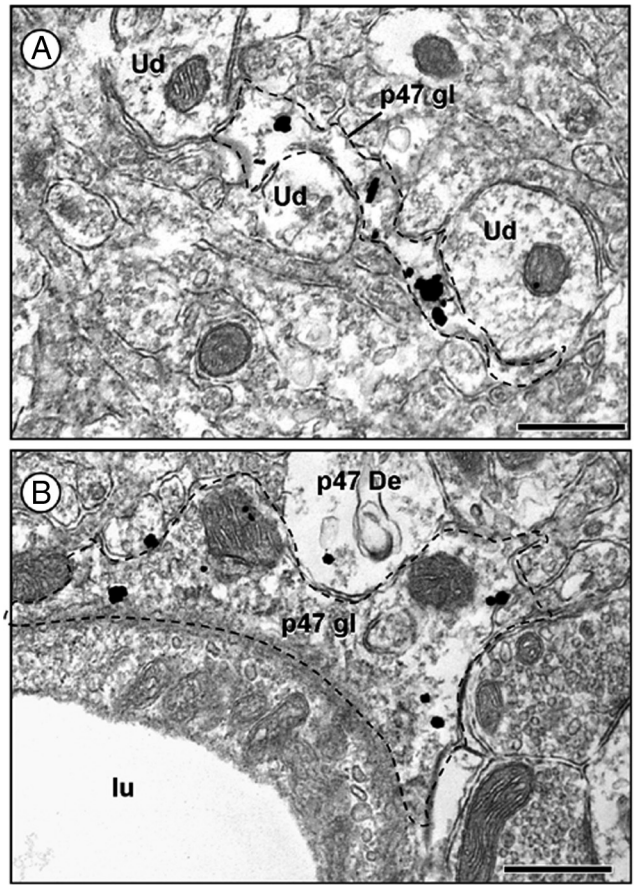

Figure 4. p47 ^{phox} immunogold particles are localized to PVN glial processes. ***A***, A densely p47 ^{phox}-labeled glia (p47 gl; dashed outline) is contacting several small unlabeled dendrites (Ud) and axons. ***B***, p47 ^{phox} immunoreactivity is observed in a perivascular astrocytic process (p47 gl; dashed outline). lu, Lumen of blood vessel. Scale bar, 500 nm.

pressin. Vasopressin immunoreactivity also was occasionally found in axons (3 of 18) and axon terminals (4 of 47) containing p47 ^{phox} labeling.

The subcellular distribution of p47 ^{phox} immunogold particles in vasopressin- and non-vasopressin-containing dendrites was similar. In saline control mice, p47 ^{phox} labeling was distributed mainly in the cytoplasmic compartment of dendrites with <18% of p47 ^{phox} immunogold particles directly associated with the plasma membrane. In the cytoplasm, p47 ^{phox} labeling appeared as a single gold particle or a cluster of gold particles (Fig. 5*A*). Nineteen percent (108 of 568) of all p47 ^{phox}-labeled dendrites received asymmetric excitatory-type synaptic contacts, and 20% (113 of 568) of all p47 ^{phox}-labeled dendrites received symmetric inhibitory-type synaptic contacts. Of these p47 ^{phox}-labeled dendrites, <2% (9 of 568) received both asymmetric and symmetric synaptic inputs.

AngII chronic infusion elicits a size-dependent change in p47 ^{phox} immunolabeled dendrites

The majority of p47 ^{phox}-labeled dendrites without vasopressin were small to medium sized as determined by their average diameter. Combining single-labeled (p47 ^{phox}) dendrites from both treatment groups, cluster analysis determined that the dendrites could be divided into three groups based on size. Small dendrites (ranging from 0.2 to 0.8 μm) composed 44.5% whereas medium dendrites (ranging from 0.8 to 1.2 μm) composed 43.5% of the total number of dendrites sampled. The remaining 12% of p47 ^{phox} single-labeled dendrites were large and more variable in size (ranging from 1.2 to 2.4 μm). Cluster analysis revealed that dual-labeled (p47 ^{phox} and vasopressin) dendrites could be divided into two groups based on size. Forty-seven percent of the dual-labeled dendrites were small (ranging from 0.4 to 1.0 μm) and 53% were medium (ranging from 1.0 to1.8 μm).

After AngII administration, the non-vasopressin dendrites containing p47 ^{phox} showed size differences from controls. The mean average diameter of non-vasopressin p47 ^{phox} dendrites was significantly ($F_{(1,722)} = 4.88$; $p < 0.05$) increased after AngII (0.92 ± 0.02 μm) compared with saline controls (0.87 ± 0.01 μm). There were no changes ($F_{(1,187)} = 0.27$; $p > 0.05$) in the average diameter of dual-labeled (p47 ^{phox} and vasopressin) dendrites after AngII. These data are consistent with the trafficking of p47 ^{phox} closer to the cell body and/or a morphological change after chronic AngII administration in non-vasopressin-containing subpopulations of p47 ^{phox}-expressing neurons in the PVN.

AngII infusion opposingly alters the distribution of p47 ^{phox} in dendrites differentially expressing vasopressin

Non-vasopressin dendrites

In PVN dendrites of mice receiving saline, p47 ^{phox} immunogold particles were commonly observed in the cytoplasm (Fig. 5*A*), whereas in dendrites of AngII-treated mice, p47 ^{phox} gold particles were frequently observed in contact with endomembranes located just beneath the plasma membrane (Fig. 5*B*,*C*). These membrane-associated p47 ^{phox} particles were often seen near portions of the plasmalemmal surface receiving synaptic input from axon terminals. Compared with controls, significantly [$\chi^2(1) = 5.29$; $p < 0.05$] more p47 ^{phox} immunogold particles contacted endomembranes in medium/large dendrites after AngII treatment (Fig. 5*D*). A small increase in endomembrane-associated p47 ^{phox} was also noted in small dendrites after AngII, but this increase was not significant [$\chi^2(1) = 0.85$; $p > 0.05$]. In addition to enhanced endomembrane association, p47 ^{phox} gold particles were found closer to the plasma membrane after chronic AngII administration compared with controls. The average p47 ^{phox} gold particle distance from the plasma membrane was decreased ($F_{(1,1687)} = 6.47$; $p = 0.01$) from 0.20 ± 0.01 μm after saline to 0.18 ± 0.01 μm after AngII administration.

Treatment-specific differences between mice receiving AngII versus saline were observed in the medium-sized dendrites only. Compared with saline, mice receiving systemic AngII showed a significant ($F_{(1,314)} = 7.75$; $p < 0.01$) decrease in cytoplasmic density of p47 ^{phox} immunogold particles (Fig. 5*E*). The p47 ^{phox} immunogold density close to the plasma membrane (<70 nm) was increased ($F_{(1,314)} = 5.24$; $p < 0.05$) after AngII compared with saline controls (Fig. 5*F*). There were no changes in plasma membrane-associated ($F_{(1,314)} = 0.17$; $p > 0.05$; Fig. 5*G*) or total p47 ^{phox} immunogold density ($F_{(1,314)} = 0.97$; $p > 0.05$; Fig. 5*H*) in non-vasopressin dendrites after AngII administration.

Vasopressin dendrites

Compared with controls (Fig. 6*A*), p47 ^{phox} gold particles were less frequently found on the plasma membrane after chronic AngII infusion (Fig. 6*B*). Because of the dark peroxidase immunoreaction product identifying vasopressin-containing dendrites, it was difficult to visualize small endomembrane structures. Therefore, we were unable to determine the p47 ^{phox} gold particle associations with endomembranes in the vasopressin-containing dendrites of saline- and AngII-treated mice. However, the average p47 ^{phox} gold particle distance from the plasmalemmal surface

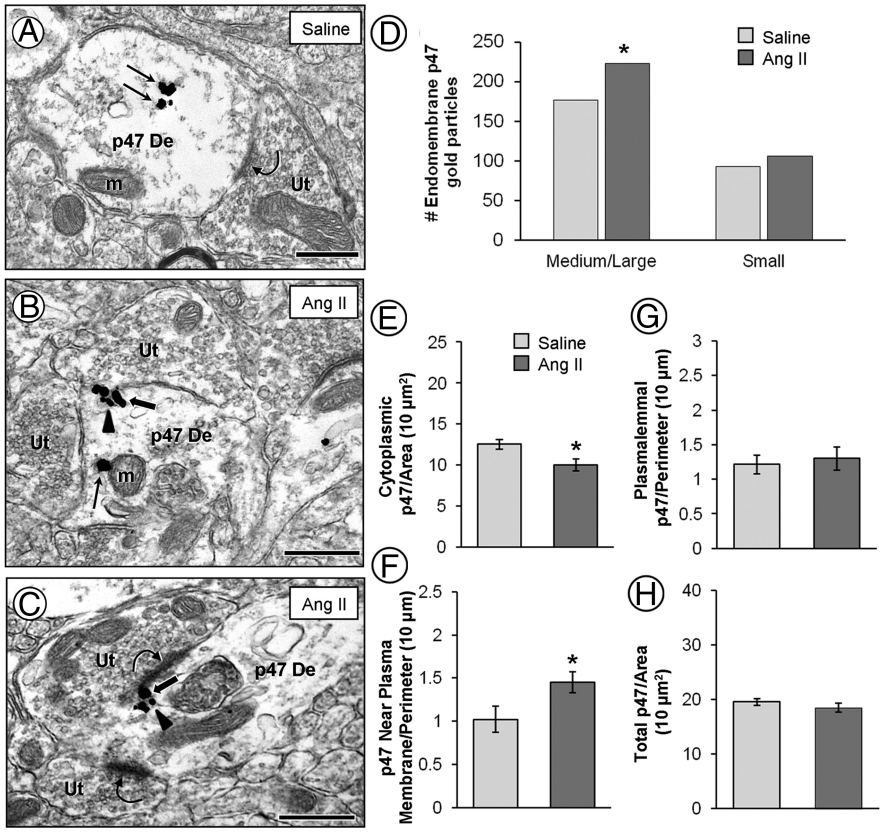

Figure 5. Electron micrographs (***A–C***) and quantitative analysis (bar graphs, ***D–H***) showing p47 ^{phox} immunogold particles in dendrites without vasopressin the PVN. Non-vasopressin dendrites (p47 De) have a predominantly cytoplasmic distribution (straight arrows) of p47 ^{phox} immunogold particles in saline recipient mice (***A***). After AngII infusion, p47 ^{phox} immunogold particles are more often seen just beneath the plasma membrane (block arrows), associated with small endomembranous structures (arrowheads) (***B***, ***C***). Many of the p47 ^{phox} clusters of immunogold particles were observed near asymmetric excitatory-type synapses (curved arrows). The bar graphs show a significant increase in endomembrane-associated p47 ^{phox} in medium/large, but not small, dendrites after AngII (***D***). There is also a significant decrease in p47 ^{phox} cytoplasmic density (***E***) with a corresponding increase in p47 ^{phox} density near the plasma membrane (***F***) compared with saline controls. No significant differences are found between the AngII group and saline controls in p47 ^{phox} plasmalemmal (***G***) and total (***H***) density. Ut, Unlabeled terminal; m, mitochondria. *$p < 0.05$. Scale bar, 500 nm.

was significantly ($F_{(1,478)} = 6.05$; $p < 0.05$) increased in vasopressin-containing dendrites of mice receiving AngII (0.25 ± 0.01 μm) compared with saline controls (0.21 ± 0.01 μm).

A between-group difference in dendritic plasmalemmal ($F_{(1,187)} = 4.048$; $p < 0.05$) and total ($F_{(1,187)} = 10.220$; $p < 0.05$) p47 ^{phox} labeling was found in vasopressin-labeled dendrites. Compared with saline controls, mice administered AngII showed a decrease in the plasmalemmal (Fig. 6*E*) and total (Fig. 6*F*) density of p47 ^{phox} immunogold. There were no between-group differences in the cytoplasmic density ($F_{(1,187)} = 2.881$; $p > 0.05$; Fig. 6*C*) or p47 ^{phox} immunogold particle density <70 nm from the plasma membrane ($F_{(1,187)} = 2.364$; $p > 0.05$; Fig. 6*D*).

Discussion

Our results provide new evidence that slow-pressor AngII is accompanied by enhanced NOX2-dependent ROS signaling that differentially occurs in subpopulations of PVN neurons distinguished by their content of vasopressin. We found that dendrites of both vasopressin and non-vasopressin neurons in the PVN contain p47 ^{phox}. However, after 14 d of chronic low-dose AngII, only the non-vasopressin dendrites in this brain region showed trafficking of p47 ^{phox} to sites near the plasmalemma, which were identified as endomembranes. This surface membrane trafficking is consistent with NADPH oxidase complex assembly and activation and with the increased baseline ROS seen exclusively in isolated neurons without detectable VP–eGFP. In contrast, there was a significant reduction in dendritic plasmalemmal and total density of p47 ^{phox} in the AngII-infused mice, which also failed to show an effect of systemic AngII infusion on ROS fluorescence, in isolated VP–eGFP neurons. However, NMDA-induced ROS was significantly increased in both non-VP–eGFP and VP–eGFP neurons isolated from the mice showing AngII-induced slow-pressor hypertension. These observations suggest that this type of hypertension is linked with dysregulation of cardiovascular homeostasis resulting from differential changes in NADPH oxidase-dependent free radical production in non-vasopressin and vasopressin neurons in the PVN.

Somatodendritic labeling of p47 ^{phox} in the PVN

Within somata and dendrites under control conditions, p47 ^{phox} immunoreactivity was found in the cytoplasm near or contacting intracellular organelles and was also observed, to a lesser extent, on synaptic and extrasynaptic portions of the plasma membrane. The association of p47 ^{phox} with endomembranes resembling endoplasmic reticulum is consistent with the role of these structures in protein transport and calcium signaling (Glass et al., 2007). Many of these endoplasmic reticula-like structures were in close contact with the outer membrane of mitochondria. The endoplasmic reticulum–mitochondrial matrix is the target of many proteins, likely because of the tethering of these two organelles and the generation of calcium microdomains (Bakowski et al., 2012). NADPH oxidase enzymes require calcium for activation. Intracellular Ca^{2+} activates phosphokinase, which in turn phosphorylates p47 ^{phox}, stimulating its translocation to membranes along with other NADPH oxidase subunits to assemble the activated enzyme complex (Bedard and Krause, 2007). Conversely, intracellular Ca^{2+} is regulated by NADPH oxidase. In neurons, NADPH oxidase-derived ROS increases Ca^{2+} influx by increasing the opening of voltage-dependent L-type Ca^{2+} channels (Zimmerman et al., 2005; Wang et al., 2006). Furthermore, NADPH oxidase-derived ROS in other cell types induces Ca^{2+} release from intracellular stores, involving activation of ryanodine and/or inositol triphosphate receptors (Bedard and Krause, 2007). Together along with the present findings, a close physical interaction may exist between NADPH oxidase subunit p47 ^{phox} and intracellular Ca^{2+} storage sites that would allow for the rapid generation of ROS and optimal regulation of calcium-dependent signaling pathways.

AngII-induced trafficking of p47 ^{phox} in non-vasopressin-containing dendrites accompanies ROS production in the PVN

In non-vasopressin-containing PVN dendrites, we found that slow-pressor AngII evoked p47 ^{phox} trafficking, resulting in an

enhanced association of p47^{phox} with membranous structures near the plasmalemmal surface. Moreover, this subcellular redistribution of p47^{phox} was accompanied by an increase in ROS production in non-vasopressin neurons of the PVN. These results are consistent with Erdös et al. (2006), whose findings support a role for NADPH oxidase-derived ROS in the PVN using acute AngII administration. In the cortex and brainstem, gp91^{phox} is found in dendrites on the plasma membrane and nearby smooth endoplasmic reticulum (Wang et al., 2004; Glass et al., 2006; Girouard et al., 2009), locations similar to where we presently observed an accumulation of p47^{phox} in PVN dendrites of mice receiving AngII. Thus, the present findings provide strong ultrastructural evidence for increased assembly of functional NADPH oxidase in non-vasopressin neurons of the PVN in response to slow-pressor AngII.

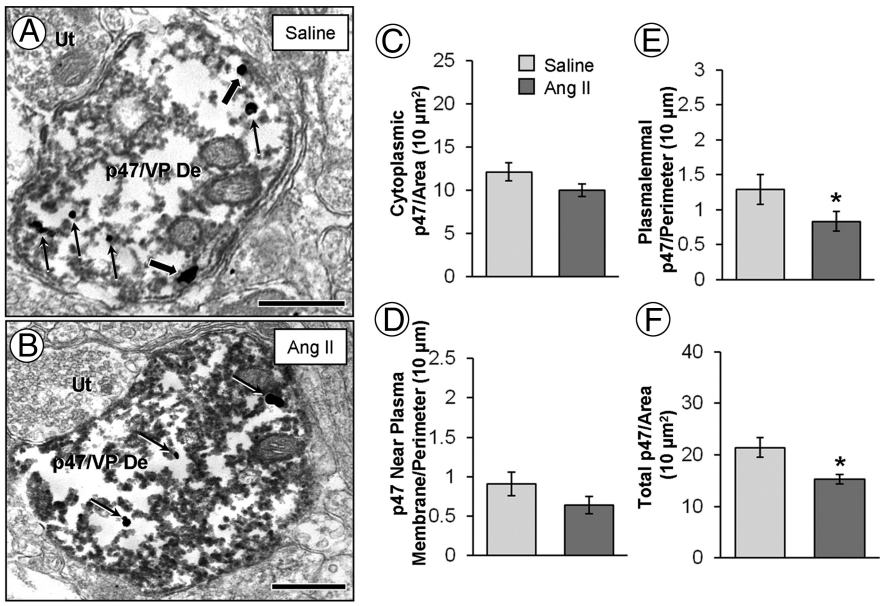

Figure 6. Electron micrographs (***A***, ***B***) and quantitative analysis (bar graphs, ***C–F***) showing p47^{phox} immunogold particles in dendrites containing immunoperoxidase labeling for vasopressin in the PVN. In vasopressin-labeled dendrites (p47/VP De) of saline recipient mice, p47^{phox} is found both in the cytoplasm (straight arrows) and on the plasma membrane (block arrows; ***A***). After AngII, p47^{phox} gold particles are less frequently found on the plasma membrane (***B***). The bar graphs show no significant differences between the AngII group and saline controls in p47^{phox} cytoplasmic (***C***) and near plasmalemmal (***D***) density. However, there is a significant decrease in p47^{phox} plasmalemmal (***E***) and total (***F***) density. Ut, Unlabeled terminal. *$p < 0.05$. Scale bar, 500 nm.

A neuronal source of ROS production is indicated by our imaging results in isolated PVN neurons, showing an elevation in both baseline and NMDA-evoked superoxide after chronic systemic administration of a subpressor dose of AngII. However, p47^{phox} immunoreactivity was observed in both neuronal and glial processes throughout the PVN, which is consistent with the distribution of NADPH oxidase subunits described previously in other brain regions (Abramov et al., 2005; Glass et al., 2006; Glass et al., 2007; Chéret et al., 2008; Sorce and Krause, 2009). Thus, non-neuronal cells, such as astroglia and/or microglia, also may contribute to ROS production in the PVN.

Although the central mechanisms regulating the effects of systemic AngII on the PVN are not fully understood, circulating AngII acting on the circumventricular subfornical organ (SFO) is a likely upstream mediator of the ROS response in the PVN. Activation of AT1 receptors by AngII in the SFO induces local production of ROS (Peterson et al., 2006). Changes in calcium homeostasis, as a result of enhanced ROS in the SFO, are thought to increase activation of glutamatergic SFO neurons projecting to the PVN (Bains and Ferguson, 1995; Benarroch, 2005; Zimmerman et al., 2005). Similarly, increased ROS in the PVN may enhance the activation of descending sympathoregulatory neurons, thereby contributing to the hypertensive effect observed with slow-pressor AngII.

Systemic AngII elicits a dichotomous change in dendritic expression of p47^{phox} and NMDA-evoked ROS production in vasopressin neurons in the PVN

Recent studies by Capone et al. (2012) have shown that slow-pressor AngII increases vasopressin immunoreactivity in the PVN and elevates plasma vasopressin after 14 d, a time point when ROS is significantly increased in the PVN as demonstrated in the present study. We also saw an increase in NMDA-evoked, but not baseline, production of ROS in VP–eGFP neurons isolated from mice showing slow-pressor AngII-induced hypertension. The discharge rate of vasopressin neurons is responsive to NMDA application (Iremonger et al., 2010), and glutamate NMDA receptor signaling is highly implicated in NADPH oxidase-derived ROS production (Brennan et al., 2009; Girouard et al., 2009). This may provide one of the key mechanisms by which SFO input increases vasopressin release in response to ventricular or systemic injection of AngII (Iovino and Steardo, 1984; Mangiapane et al., 1984).

The failure to observe an increase in baseline ROS in the isolated VP–eGFP neurons in mice showing AngII-induced slow-pressor hypertension is consistent with the reduction in total and plasmalemma-associated p47^{phox} in vasopressin dendrites and NOX2-dependent ROS production in these cells. However, these effects on p47^{phox} are more difficult to reconcile with the increased NMDA-induced ROS in VP–eGFP neurons of mice receiving systemic AngII. Conceivably, the chronic infusion of subpressor AngII may produce activation of glutamatergic inputs to vasopressin neurons in the PVN, thus potentiating NMDA receptor-mediated glutamatergic transmission. Vasopressin neurons in the PVN receive a particularly dense glutamatergic innervation (van den Pol et al., 1990; Iremonger et al., 2010), mostly provided by the AngII-activated SFO. The augmented NMDA receptor-mediated influx of calcium could significantly alter the calcium-dependent translocation of p47^{phox} as has been shown for trafficking of other related proteins (Sturgill et al., 2009).

Conclusion

Our results suggest that differential free radical production in non-vasopressin and vasopressin neurons in the PVN contributes to slow-pressor AngII hypertension. Our findings are consistent with increased ROS production (AngII and NMDA) by NADPH oxidases dependent on p47^{phox} (NOX1, NOX2) in non-vasopressin neurons and NADPH oxidases not dependent on

p47^{phox} (e.g., NOX4) (Sedeek et al., 2009) and mitochondria (Daiber, 2010) in vasopressin neurons. Future studies will assess this possibility.

References

Abramov AY, Jacobson J, Wientjes F, Hothersall J, Canevari L, Duchen MR (2005) Expression and modulation of an NADPH oxidase in mammalian astrocytes. J Neurosci 25:9176–9184. CrossRef Medline

Bains JS, Ferguson AV (1995) Paraventricular nucleus neurons projecting to the spinal cord receive excitatory input from the subfornical organ. Am J Physiol 268:R625–R633. Medline

Bakowski D, Nelson C, Parekh AB (2012) Endoplasmic reticulum-mitochondria coupling: local Ca(2+) signalling with functional consequences. Pflugers Arch 464:27–32. CrossRef Medline

Bedard K, Krause KH (2007) The NOX family of ROS-generating NADPH oxidases: physiology and pathophysiology. Physiol Rev 87:245–313. CrossRef Medline

Benarroch EE (2005) Paraventricular nucleus, stress response, and cardiovascular disease. Clin Auton Res 15:254–263. CrossRef Medline

Biag J, Huang Y, Gou L, Hintiryan H, Askarinam A, Hahn JD, Toga AW, Dong HW (2012) Cyto- and chemoarchitecture of the hypothalamic paraventricular nucleus in the C57BL/6J male mouse: a study of immunostaining and multiple fluorescent tract tracing. J Comp Neurol 520:6–33. CrossRef Medline

Braga VA, Medeiros IA, Ribeiro TP, França-Silva MS, Botelho-Ono MS, Guimarães DD (2011) Angiotensin-II-induced reactive oxygen species along the SFO-PVN-RVLM pathway: implications in neurogenic hypertension. Braz J Med Biol Res 44:871–876. CrossRef Medline

Brennan AM, Suh SW, Won SJ, Narasimhan P, Kauppinen TM, Lee H, Edling Y, Chan PH, Swanson RA (2009) NADPH oxidase is the primary source of superoxide induced by NMDA receptor activation. Nat Neurosci 12:857–863. CrossRef Medline

Capone C, Faraco G, Park L, Cao X, Davisson RL, Iadecola C (2011) The cerebrovascular dysfunction induced by slow pressor doses of angiotensin II precedes the development of hypertension. Am J Physiol Heart Circ Physiol 300:H397–H407. CrossRef Medline

Capone C, Faraco G, Peterson JR, Coleman C, Anrather J, Milner TA, Pickel VM, Davisson RL, Iadecola C (2012) Central cardiovascular circuits contribute to the neurovascular dysfunction in angiotensin II hypertension. J Neurosci 32:4878–4886. CrossRef Medline

Chéret C, Gervais A, Lelli A, Colin C, Amar L, Ravassard P, Mallet J, Cumano A, Krause KH, Mallat M (2008) Neurotoxic activation of microglia is promoted by a nox1-dependent NADPH oxidase. J Neurosci 28:12039–12051. CrossRef Medline

Coleman CG, Wang G, Park L, Anrather J, Delagrammatikas GJ, Chan J, Zhou J, Iadecola C, Pickel VM (2010) Chronic intermittent hypoxia induces NMDA receptor-dependent plasticity and suppresses nitric oxide signaling in the mouse hypothalamic paraventricular nucleus. J Neurosci 30:12103–12112. CrossRef Medline

Daiber A (2010) Redox signaling (cross-talk) from and to mitochondria involves mitochondrial pores and reactive oxygen species. Biochim Biophys Acta 1797:897–906. CrossRef Medline

de Wardener HE (2001) The hypothalamus and hypertension. Physiol Rev 81:1599–1658. Medline

Drouyer E, LeSauter J, Hernandez AL, Silver R (2010) Specializations of gastrin-releasing peptide cells of the mouse suprachiasmatic nucleus. J Comp Neurol 518:1249–1263. CrossRef Medline

Erdös B, Broxson CS, King MA, Scarpace PJ, Tümer N (2006) Acute pressor effect of central angiotensin II is mediated by NAD(P)H-oxidase-dependent production of superoxide in the hypothalamic cardiovascular regulatory nuclei. J Hypertens 24:109–116. CrossRef Medline

Girouard H, Wang G, Gallo EF, Anrather J, Zhou P, Pickel VM, Iadecola C (2009) NMDA receptor activation increases free radical production through nitric oxide and NOX2. J Neurosci 29:2545–2552. CrossRef Medline

Glass MJ, Huang J, Oselkin M, Tarsitano MJ, Wang G, Iadecola C, Pickel VM (2006) Subcellular localization of nicotinamide adenine dinucleotide phosphate oxidase subunits in neurons and astroglia of the rat medial nucleus tractus solitarius: relationship with tyrosine hydroxylase immunoreactive neurons. Neuroscience 143:547–564. CrossRef Medline

Glass MJ, Chan J, Frys KA, Oselkin M, Tarsitano MJ, Iadecola C, Pickel VM (2007) Changes in the subcellular distribution of NADPH oxidase subunit p47phox in dendrites of rat dorsomedial nucleus tractus solitarius neurons in response to chronic administration of hypertensive agents. Exp Neurol 205:383–395. CrossRef Medline

Gong S, Zheng C, Doughty ML, Losos K, Didkovsky N, Schambra UB, Nowak NJ, Joyner A, Leblanc G, Hatten ME, Heintz N (2003) A gene expression atlas of the central nervous system based on bacterial artificial chromosomes. Nature 425:917–925. CrossRef Medline

Gonzalez AD, Wang G, Waters EM, Gonzales KL, Speth RC, Van Kempen TA, Marques-Lopes J, Young CN, Butler SD, Davisson RL, Iadecola C, Pickel VM, Pierce JP, Milner TA (2012) Distribution of angiotensin type 1a receptor-containing cells in the brains of bacterial artificial chromosome transgenic mice. Neuroscience 226:489–509. CrossRef Medline

Infanger DW, Sharma RV, Davisson RL (2006) NADPH oxidases of the brain: distribution, regulation, and function. Antioxid Redox Signal 8:1583–1596. CrossRef Medline

Iovino M, Steardo L (1984) Vasopressin release to central and peripheral angiotensin II in rats with lesions of the subfornical organ. Brain Res 322:365–368. CrossRef Medline

Iremonger KJ, Benediktsson AM, Bains JS (2010) Glutamatergic synaptic transmission in neuroendocrine cells: basic principles and mechanisms of plasticity. Front Neuroendocrinol 31:296–306. CrossRef Medline

Jones SA, Wood JD, Coffey MJ, Jones OT (1994) The functional expression of p47-phox and p67-phox may contribute to the generation of superoxide by an NADPH oxidase-like system in human fibroblasts. FEBS Lett 355:178–182. CrossRef Medline

Kang YM, Ma Y, Zheng JP, Elks C, Sriramula S, Yang ZM, Francis J (2009) Brain nuclear factor-kappa B activation contributes to neurohumoral excitation in angiotensin II-induced hypertension. Cardiovasc Res 82:503–512. CrossRef Medline

Kawada N, Imai E, Karber A, Welch WJ, Wilcox CS (2002) A mouse model of angiotensin II slow pressor response: role of oxidative stress. J Am Soc Nephrol 13:2860–2868. CrossRef Medline

Kc P, Balan KV, Tjoe SS, Martin RJ, Lamanna JC, Haxhiu MA, Dick TE (2010) Increased vasopressin transmission from the paraventricular nucleus to the rostral medulla augments cardiorespiratory outflow in chronic intermittent hypoxia-conditioned rats. J Physiol 588:725–740. CrossRef Medline

Keil LC, Summy-Long J, Severs WB (1975) Release of vasopressin by angiotensin II. Endocrinology 96:1063–1065. CrossRef Medline

Kunz A, Anrather J, Zhou P, Orio M, Iadecola C (2007) Cyclooxygenase-2 does not contribute to postischemic production of reactive oxygen species. J Cereb Blood Flow Metab 27:545–551. CrossRef Medline

Lane DA, Lessard AA, Chan J, Colago EE, Zhou Y, Schlussman SD, Kreek MJ, Pickel VM (2008) Region-specific changes in the subcellular distribution of AMPA receptor GluR1 subunit in the rat ventral tegmental area after acute or chronic morphine administration. J Neurosci 28:9670–9681. CrossRef Medline

Mangiapane ML, Thrasher TN, Keil LC, Simpson JB, Ganong WF (1984) Role for the subfornical organ in vasopressin release. Brain Res Bull 13:43–47. CrossRef Medline

Milner TA, Waters EM, Robinson DC, Pierce JP (2011) Degenerating processes identified by electron microscopic immunocytochemical methods. Methods Mol Biol 793:23–59. CrossRef Medline

Oliveira-Sales EB, Nishi EE, Carillo BA, Boim MA, Dolnikoff MS, Bergamaschi CT, Campos RR (2009) Oxidative stress in the sympathetic premotor neurons contributes to sympathetic activation in renovascular hypertension. Am J Hypertens 22:484–492. CrossRef Medline

Paxinos G, Franklin KBJ, eds (2001) The mouse brain in stereotaxic coordinates. San Diego: Academic.

Peters A, Palay SL, Webster H, eds (1991) The fine structure of the nervous system. New York: Oxford UP.

Peterson JR, Sharma RV, Davisson RL (2006) Reactive oxygen species in the neuropathogenesis of hypertension. Curr Hypertens Rep 8:232–241. CrossRef Medline

Qi J, Zhang DM, Suo YP, Song XA, Yu XJ, Elks C, Lin YX, Xu YY, Zang WJ, Zhu Z, Kang YM (2013) Renin-angiotensin system modulates neurotransmitters in the paraventricular nucleus and contributes to angiotensin II-induced hypertensive response. Cardiovasc Toxicol 13:48–54. CrossRef Medline

Rothe G, Valet G (1990) Flow cytometric analysis of respiratory burst activity in phagocytes with hydroethidine and 2′,7′-dichlorofluorescin. J Leukoc Biol 47:440–448. Medline

Sedeek M, Hébert RL, Kennedy CR, Burns KD, Touyz RM (2009) Molecular mechanisms of hypertension: role of Nox family NADPH oxidases. Curr Opin Nephrol Hypertens 18:122–127. CrossRef Medline

Sorce S, Krause KH (2009) NOX enzymes in the central nervous system: from signaling to disease. Antioxid Redox Signal 11:2481–2504. CrossRef Medline

Sturgill JF, Steiner P, Czervionke BL, Sabatini BL (2009) Distinct domains within PSD-95 mediate synaptic incorporation, stabilization, and activity-dependent trafficking. J Neurosci 29:12845–12854. CrossRef Medline

van den Pol AN, Wuarin JP, Dudek FE (1990) Glutamate, the dominant excitatory transmitter in neuroendocrine regulation. Science 250: 1276–1278. CrossRef Medline

Veltmar A, Culman J, Qadri F, Rascher W, Unger T (1992) Involvement of adrenergic and angiotensinergic receptors in the paraventricular nucleus in the angiotensin II-induced vasopressin release. J Pharmacol Exp Ther 263:1253–1260. Medline

Wang G, Anrather J, Huang J, Speth RC, Pickel VM, Iadecola C (2004) NADPH oxidase contributes to angiotensin II signaling in the nucleus tractus solitarius. J Neurosci 24:5516–5524. CrossRef Medline

Wang G, Anrather J, Glass MJ, Tarsitano MJ, Zhou P, Frys KA, Pickel VM, Iadecola C (2006) Nox2, Ca^{2+}, and protein kinase C play a role in angiotensin II-induced free radical production in nucleus tractus solitarius. Hypertension 48:482–489. CrossRef Medline

Zimmerman MC, Sharma RV, Davisson RL (2005) Superoxide mediates angiotensin II-induced influx of extracellular calcium in neural cells. Hypertension 45:717–723. CrossRef Medline